

Intrinsic Sliced Wasserstein Distances for Comparing Collections of Probability Distributions on Manifolds and Graphs

Raif M. Rustamov and Subhabrata Majumdar

Data Science and AI Research, AT&T Chief Data Office, USA

Abstract

Collections of probability distributions arise in a variety of statistical applications ranging from user activity pattern analysis to brain connectomics. In practice these distributions are represented by histograms over diverse domain types including finite intervals, circles, cylinders, spheres, other manifolds, and graphs. This paper introduces an approach for detecting differences between two collections of histograms over such general domains. To this end, we introduce the intrinsic slicing construction that yields a novel class of Wasserstein distances on manifolds and graphs. These distances are Hilbert embeddable, which allows us to reduce the histogram collection comparison problem to the comparison of means in a high-dimensional Euclidean space. We develop a hypothesis testing procedure based on conducting t -tests on each dimension of this embedding, then combining the resulting p -values using recently proposed p -value combination techniques. Our numerical experiments in a variety of data settings show that the resulting tests are powerful and the p -values are well-calibrated. Example applications to user activity patterns, spatial data, and brain connectomics are provided.

1 Introduction

Histograms serve as an overarching representation of distributional data in a variety of statistical applications. An important aspect is that in practice these are not limited to histograms over real intervals, but are often defined over manifolds and graphs. For instance, even in the simplest case of analyzing 24-hour activity patterns, the resulting histograms are really supported on a circle rather than an interval on the real line. If in addition to the time of activity, the observations come with a real number such as the intensity of the activity, then we end up with a histogram over a cylindrical domain. Spatial datasets that are recorded at some geographic region level provide another example: one can build a histogram over the region adjacency graph by capturing the normalized counts of events in each region. When analyzing histograms over such general domains it is desirable to rely on methods that take into account the connectivity and geometry of the histogram domain, respect the distributional nature of the data, and lead to efficient practical algorithms.

In this paper we consider the problem of comparing two collections of histograms, namely testing whether they “agree on average”. To exemplify this type of a problem, consider histograms over finite interval that were collected for two groups of people. For simplicity, we can think of histograms as curves over the interval—a familiar setting in functional data analysis [34]. The objective of the hypothesis test is to determine whether the “average curves” of the two curve collections are the same. Our goal is to be able to conduct such tests for collections of histograms defined over manifolds and graphs. A test like this would be useful in numerous practical situations. For instance, an online retailer may aggregate monthly customer activity into a histogram

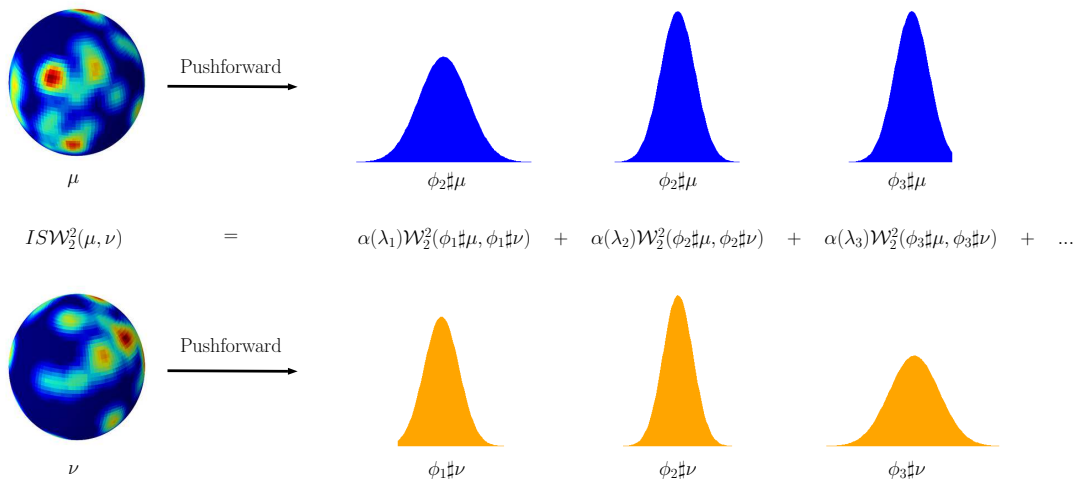


Figure 1: Schematic of the proposed intrinsic slicing construction. Given two probability measures on the sphere (here the darkest blue corresponds to zero mass), different aspects of their dissimilarities become apparent after pushforward to the real line using the eigenfunctions of the Laplace-Beltrami operator, $\{\phi_i\}$, in this case spherical harmonics. As a particular example of our general construction, the (squared) intrinsic sliced 2-Wasserstein distance $ISW_2^2(\cdot, \cdot)$ is the weighted sum of the dissimilarities of the corresponding pushforwards of μ and ν as measured by squared 2-Wasserstein distance $W_2^2(\cdot, \cdot)$ on the real line.

over a cylinder capturing the time of the day and amount of purchase for each transaction. By considering collections of histograms for various customer segments, one can conduct tests to determine if there are statistically significant differences between average patterns of these segments.

The functional data analysis analogy above is helpful for grasping the problem, yet the distributional nature of the histogram data requires dedicated methodology (see e.g. [32, 27] for particular examples). For example, bin-wise treatment of histograms may result in increased variability when horizontal variation is present, leading eventually to less powerful methods. Transportation based distances between probability distributions are more efficient at capturing this and other aspects of distributional data [26, 28, 4]. Adopting the transportation theoretic approaches to our problem—particularly the notion of Fréchet mean for averaging the distributions—immediately hits a roadblock beyond the real line case. While Fréchet mean has been at the center of the recent progress in adapting the traditional statistical approaches to the settings of manifolds and graphs, such as PCA [12, 7], analysis of variance (ANOVA) [13], and regression [9], it has a number of shortcomings. On general domains, the existence and uniqueness of the Fréchet mean is not guaranteed, and it can be sensitive to small changes in the distributions. Regularization may help with these issues, yet computing the Fréchet mean is computationally expensive and becomes prohibitive when resampling is used to construct the null distribution for hypothesis testing.

In this work we overcome these difficulties by formulating a rigorous definition of “agreement on average” via Hilbertian distances and corresponding Hilbert embeddings of distributions, which avoids the stability and uniqueness issues associated with the Fréchet mean. While 2-Wasserstein distance on the real line is Hilbert embeddable, it fails to be so on general domains [28]. Inspired by the sliced 2-Wasserstein distances in high dimensional spaces [21, 20], we introduce a new slicing construction (Figure 1) that leverages the eigenvalues and eigenfunctions of the Laplace-

Beltrami operator on manifolds and of the Laplacian on graphs to capture the intrinsic geometry and connectivity of the domain. We apply this slicing construction to obtain a novel class of intrinsic sliced 2-Wasserstein distances on manifolds and graphs. The resulting distances are Hilbert embeddable, which allows us to reduce the histogram collection comparison problem to the comparison of means in a high-dimensional Euclidean space. Hypothesis testing is performed by conducting t -tests on each dimension of the embedding and combining the resulting p -values using recently introduced p -value combination techniques that are robust to dependencies [15, 35, 24]. We verify via simulations and real examples in a variety of data settings that the resulting tests are powerful, and the p -values are well-calibrated.

Our work is in line with recent developments that utilize Hilbert embeddings for simplifying distributional problems. It was noted early on that the expression for 2-Wasserstein distance on the real line in terms of quantiles (c.f. [8]) gives rise to a straightforward Hilbert embedding. A more general Hilbert embedding framework with a number of concrete constructions was provided in [27]. However, these are not tied to a distance between probability distributions and so can be problematic for capturing the variability of a collection of distributions. In addition, [27] has difficulties in higher dimensions and does not provide constructions suitable for manifolds or graphs.

The paper is organized as follows. We introduce the theoretical machinery for our framework, and go over the rigorous definition of our testing problem in Section 2. The case of the finite intervals on the real line can be treated directly using the 2-Wasserstein distance and is presented in a dedicated Section 2.3 due to its importance. To tackle the case of general domains we introduce the intrinsic slicing construction and the resulting distances in Section 3. Next, we go over the practical details of hypothesis testing on manifolds and graphs in Section 4. Finally, we present simulation results and real data analyses in Section 5.

2 Preliminaries

2.1 Hilbert Embeddings and Agreement on Average

Given a compact metric space \mathcal{X} , let $\mathcal{P}(\mathcal{X})$ denote the set of Borel probability measures on \mathcal{X} . Our main interest is in the case where \mathcal{X} is a graph or a manifold with the shortest/geodesic distance as the metric, and thus the compactness restriction. Histograms can be represented as discrete measures of the form $\sum_a w_a \delta_{x_a}$ with the histogram bin centers $x_a \in \mathcal{X}$ and non-negative weights w_a satisfying $\sum_a w_a = 1$; here δ_x is the delta measure supported at x . In practice we will always be working with histograms, but our theoretical developments are general and will be presented using measure-theoretic terminology. In what follows, we may refer to a histogram as a probability measure or probability distribution. We reserve the term histogram for discrete measures, and use it to stress discreteness or to discuss practical aspects of our methodology.

The 2-Wasserstein distance can be defined on $\mathcal{P}(\mathcal{X})$ using the metric of \mathcal{X} as the ground distance [28, 26], giving $\mathcal{W}_2^{\mathcal{X}} : \mathcal{P}(\mathcal{X}) \times \mathcal{P}(\mathcal{X}) \rightarrow \mathbb{R}_{\geq 0}$; due to the repeated use of the real line case we use the shorthand $\mathcal{W}_2 = \mathcal{W}_2^{\mathbb{R}}$. Central to our study are distributions on the space of probability measures $\mathcal{P}(\mathcal{P}(\mathcal{X})) = (\mathcal{P}(\mathcal{X}), \mathcal{B}(\mathcal{P}(\mathcal{X})))$, where $\mathcal{B}(\mathcal{P}(\mathcal{X}))$ is the Borel σ -algebra generated by the topology induced by $\mathcal{W}_2^{\mathcal{X}}$ [4]. Let $P, Q \in \mathcal{P}(\mathcal{P}(\mathcal{X}))$, and assume that we are given two collections of probability measures $\{\mu_i\}_{i=1}^{N_1}$ and $\{\nu_i\}_{i=1}^{N_2}$ that are drawn from P and Q : $\mu_i \sim P$ and $\nu_i \sim Q$ in an independent-and-identically-distributed (hereafter i.i.d.) manner. Our goal is to use this sample to test the null hypothesis of whether P and Q agree on average—a notion that we formalize next.

Let $\mathcal{D}(\cdot, \cdot) : \mathcal{P}(\mathcal{X}) \times \mathcal{P}(\mathcal{X}) \rightarrow \mathbb{R}_{\geq 0}$ be a *Hilbertian* distance between probability distributions [28]. This means that there exist a Hilbert space \mathcal{H} and a map $\eta : \mathcal{P}(\mathcal{X}) \rightarrow \mathcal{H}$ such that

$\mathcal{D}(\mu, \nu) = \|\eta(\mu) - \eta(\nu)\|_{\mathcal{H}}$. For example, it is well-known that 2-Wasserstein distance on $\mathcal{X} = \mathbb{R}$ is Hilbertian (also see Section 2.3) and Maximum Mean Discrepancy (MMD) [17] on any \mathcal{X} is Hilbertian.

Definition 1. Two distributions on the space of probability measures $P, Q \in \mathcal{P}(\mathcal{P}(\mathcal{X}))$ are said to *agree on average* with respect to a Hilbertian distance \mathcal{D} if the following holds:

$$\mathbb{E}_{\mu \sim P}[\eta(\mu)] = \mathbb{E}_{\nu \sim Q}[\eta(\nu)], \quad (2.1)$$

where η is the Hilbert map of \mathcal{D} .

Intuitively, each “dimension” of the map η probes some aspect of the two involved processes and makes sure that they are in agreement in expectation.

Example 1. Consider the case when \mathcal{X} is a discrete space, $\mathcal{X} = \{x_a\}_{a=1}^A$, and so $\mathcal{P}(\mathcal{X}) = \{\sum_a w_a \delta_{x_a} : \sum_a w_a = 1, w_a \geq 0\}$. Let \mathcal{D} be the ℓ_2 -distance, namely $\mathcal{D}^2(\sum_a w_a \delta_{x_a}, \sum_a w'_a \delta_{x_a}) = \sum_a (w_a - w'_a)^2$. Clearly, the Hilbert map is given by $\eta(\sum_a w_a \delta_{x_a}) = [w_1, w_2, \dots, w_A] \in \mathbb{R}^A$. Any $P \in \mathcal{P}(\mathcal{P}(\mathcal{X}))$ can be described by a probability distribution $p(\mathbf{w})$ over the probability simplex in \mathbb{R}^A from which the weight vectors $[w_1, w_2, \dots, w_A]$ are drawn. Using the explicit form of the Hilbert map we see that two processes P and Q agree on average if and only if the corresponding distributions $p(\mathbf{w})$ and $q(\mathbf{w})$ have the same expectations in \mathbb{R}^A . \square

Example 2. Let $\mathcal{X} = [0, T] \subset \mathbb{R}$ and consider the following construction of $P \in \mathcal{P}(\mathcal{P}(\mathcal{X}))$ that gives probability distribution functions (pdf) over \mathcal{X} . We draw a function from a Gaussian process $GP(m_P(x), k_P(x, x'))$, clamp its negative values to zero (or take its square, or exponentiate— the goal being to obtain a non-negative function), and normalize to integrate to 1 to obtain a pdf $f : \mathcal{X} \rightarrow \mathbb{R}$. If \mathcal{D} is the L_2 -distance between functions, the Hilbert map η can be taken to be the identity map with $\mathcal{H} = L_2[0, T]$. Thus, agreement on average for two such processes boils down to $\forall x, \mathbb{E}_{f \sim P}[f(x)] = \mathbb{E}_{f \sim Q}[f(x)]$, which would hold true if, for example, the mean functions of the involved Gaussian processes are equal. This type of analysis would be similar to the functional data methodology, but it ignores the fact that probability distributions can potentially be analyzed more efficiently using a wider variety of distances \mathcal{D} such as the Wasserstein distances. \square

Since we may lack an explicit expression for the Hilbert map η , we provide the following equivalent characterization solely in terms of \mathcal{D} .

Proposition 1. $P, Q \in \mathcal{P}(\mathcal{P}(\mathcal{X}))$ agree on average with respect to \mathcal{D} if and only if:

$$\mathbb{T}(P, Q) = \frac{1}{2} \mathbb{E}_{\mu, \mu' \sim P}[\mathcal{D}^2(\mu, \mu')] + \frac{1}{2} \mathbb{E}_{\nu, \nu' \sim Q}[\mathcal{D}^2(\nu, \nu')] - \mathbb{E}_{\mu \sim P, \nu \sim Q}[\mathcal{D}^2(\mu, \nu)] = 0, \quad (2.2)$$

where to avoid notational clutter we use $\mathcal{D}^2(\cdot, \cdot)$ as a shorthand for $(\mathcal{D}(\cdot, \cdot))^2$.

Proof. This is a straightforward application of the “kernel trick”: using the Hilbert property of the distance we can rewrite,

$$\begin{aligned} \mathbb{T}(P, Q) &= \frac{1}{2} \mathbb{E}_{\mu, \mu' \sim P}[\|\eta(\mu) - \eta(\mu')\|_{\mathcal{H}}^2] + \frac{1}{2} \mathbb{E}_{\nu, \nu' \sim Q}[\|\eta(\nu) - \eta(\nu')\|_{\mathcal{H}}^2] - \mathbb{E}_{\mu \sim P, \nu \sim Q}[\|\eta(\mu) - \eta(\nu)\|_{\mathcal{H}}^2] \\ &= \mathbb{E}_{\mu \sim P}[\|\eta(\mu)\|_{\mathcal{H}}^2] + \mathbb{E}_{\nu \sim Q}[\|\eta(\nu)\|_{\mathcal{H}}^2] \\ &\quad + \langle \mathbb{E}_{\mu \sim P}[\eta(\mu)], \mathbb{E}_{\mu \sim P}[\eta(\mu)] \rangle_{\mathcal{H}} + \langle \mathbb{E}_{\nu \sim Q}[\eta(\nu)], \mathbb{E}_{\nu \sim Q}[\eta(\nu)] \rangle_{\mathcal{H}} \\ &\quad - \mathbb{E}_{\mu \sim P}[\|\eta(\mu)\|_{\mathcal{H}}^2] - \mathbb{E}_{\nu \sim Q}[\|\eta(\nu)\|_{\mathcal{H}}^2] - 2 \langle \mathbb{E}_{\mu \sim P}[\eta(\mu)], \mathbb{E}_{\nu \sim Q}[\eta(\nu)] \rangle_{\mathcal{H}} \\ &= \|\mathbb{E}_{\mu \sim P}[\eta(\mu)] - \mathbb{E}_{\nu \sim Q}[\eta(\nu)]\|_{\mathcal{H}}^2 = 0. \end{aligned} \quad (2.3)$$

Which gives the sought equivalence. \square

If we could invert the map η at $\mathbb{E}_{\mu \sim P}[\eta(\mu)]$, then the corresponding ‘‘average measure’’ of $P \in \mathcal{P}(\mathcal{P}(\mathcal{X}))$ can be introduced via $P_{\text{av}} = \eta^{-1}(\mathbb{E}_{\mu \sim P}[\eta(\mu)])$. It is easy to see that P_{av} satisfies the following:

$$P_{\text{av}} = \arg \min_{\rho \in \mathcal{P}(\mathcal{X})} \mathbb{E}_{\mu \sim P}[\mathcal{D}(\mu, \rho)^2],$$

which is the definition of the Fréchet mean, see for example [28]. In this setting, agreement on average boils down to having the same Fréchet means, $P_{\text{av}} = Q_{\text{av}}$. While this may seem like a more natural definition than what we gave above and would avoid the Hilbertian requirement, there is a number of problems with pursuing such an approach. First, the existence and uniqueness of the Fréchet mean is not guaranteed: for example, when \mathcal{D} is the 2-Wasserstein distance, uniqueness can fail even in the simplest cases (e.g. Dirac delta measures placed on opposite points on the circle). Second, the Fréchet mean can be sensitive to small changes in the distribution (e.g. two Dirac delta measures placed on north and south poles, and a third one placed nearby the north pole). Finally, computing the Fréchet mean is computationally expensive and can become prohibitively difficult when resampling is used to compute the null distribution for hypothesis testing. In contrast, we will show that our approach is robust and leads to computationally efficient algorithms.

Remark 1. Note that our testing focus is on the first order comparison of P and Q , and not on the more stringent equality null hypothesis of $P = Q$. The intrinsic sliced distances can be used for the latter as discussed in Section 6.

Remark 2. We compare and contrast our problem setting with the usual two-sample testing. Consider $P \in \mathcal{P}(\mathcal{P}(\mathcal{X}))$ constructed as follows. Let $\mu^* \in \mathcal{P}(\mathcal{X})$ be some fixed probability measure, and let $x_1, x_2, \dots, x_A \sim \mu^*$ be a random sample drawn according to this measure; construct a histogram summarizing this sample: $\frac{1}{A} \sum_{a=1}^A \delta_{x_a}$. To be crystal clear, $\frac{1}{A} \sum_{a=1}^A \delta_{x_a} \in \mathcal{P}(\mathcal{X})$ is then the sample drawn from P . In our testing scenario one would get the collection $\{\mu_i\}_{i=1}^{N_1}$, where each histogram is obtained via the procedure above: $\mu_i \sim P$. Similarly, consider $Q \in \mathcal{P}(\mathcal{P}(\mathcal{X}))$ of the same type based on some other fixed $\nu^* \in \mathcal{P}(\mathcal{X})$, and let $\{\nu_i\}_{i=1}^{N_2}$ the corresponding collection of histograms. Testing whether P and Q agree on average should in principle boil down to $\mu^* = \nu^*$ (which is true in the limit $A \rightarrow \infty$). When compared to the usual two-sample testing this may seem rather inefficient essentially requiring A times more samples (we have drawn resp. $N_1 A$ and $N_2 A$ samples from μ^* and ν^*). However, in our testing setup it is not assumed that the histograms in the collections come from P/Q of the above simple type (i.e. all μ_i are generated by drawing from the same underlying distribution μ^*). In fact, the target use-case for our approach is when these histograms are collected by observing *different* individuals who have their person-specific behaviors/distributions.

2.2 Hypothesis Testing

Let $\{\mu_i\}_{i=1}^{N_1}$ and $\{\nu_i\}_{i=1}^{N_2}$ be two collections of measures and $\mathcal{D}(\cdot, \cdot)$ be a Hilbertian probability distance. A straightforward approach to testing agreement on average is to use the quantity $\mathbb{T}(\cdot, \cdot)$ from Eq. (2.2) as the test statistic. To this end, one replaces the expectations by the empirical means, and excludes the diagonal terms to achieve unbiasedness:

$$\begin{aligned} \mathbb{T} \equiv \mathbb{T}(\{\mu_i\}_{i=1}^{N_1}, \{\nu_i\}_{i=1}^{N_2}) &= \frac{1}{2N_1(N_1 - 1)} \sum_{i,j:i \neq j} \mathcal{D}^2(\mu_i, \mu_j) + \frac{1}{2N_2(N_2 - 1)} \sum_{i,j:i \neq j} \mathcal{D}^2(\nu_i, \nu_j) \\ &\quad - \frac{1}{N_1 N_2} \sum_{i,j} \mathcal{D}^2(\mu_i, \nu_j). \end{aligned} \quad (2.4)$$

We will see that the map $\eta : \mathcal{P}(\mathcal{X}) \rightarrow \mathcal{H}$ can be approximated by a finite dimensional embedding $\eta_D : \mathcal{P}(\mathcal{X}) \rightarrow \mathbb{R}^D$, in the sense that $\langle \eta(\mu), \eta(\nu) \rangle_{\mathcal{H}} \approx \eta_D(\mu) \cdot \eta_D(\nu)$, where the latter is the usual dot product of vectors. Using Eq. (2.3), we obtain,

$$\mathbb{T} \approx \left\| \frac{1}{N_1} \sum_{i=1}^{N_1} \eta_D(\mu_i) - \frac{1}{N_2} \sum_{i=1}^{N_2} \eta_D(\nu_i) \right\|^2, \quad (2.5)$$

where the norm is the Euclidean norm in \mathbb{R}^D . Replacing the test statistic with this approximation leads to efficient computations by avoiding the quadratic complexity of the original statistic. This more efficient procedure can in principle be used with resampling (via randomly shuffling the distributions across the two collections) to generate the null distribution of \mathbb{T} . One issue with the resampling approach is that the granularity of the p -values is determined by the number of resamples, and can be too coarse in massive multiple comparison settings often seen in industrial applications. Therefore, we describe an alternative approach that avoids resampling.

An important observation about the formulation via Eq. (2.5) is that it can be interpreted as a two-sample mean testing in \mathbb{R}^D using the distance between the means as the test statistic. In principle, other test statistics can be used to carry out the test. Our goal is to come up with an approach that does not require resampling to compute the p -value. We closely follow the strategy proposed in [31] to obtain such a test.

Similarly to [31] we apply t -tests independently to each coordinate of the η_D -embedding and combine the resulting p -values. The validity of the t -test in our setting can be established as follows. Due to the compactness of the underlying space \mathcal{X} and the way η_D is constructed in the next section, the image of $\mathcal{P}(\mathcal{X})$ under embedding η_D is a bounded subset of \mathbb{R}^D . Concentrating on the k -th coordinate of the embedding, we see that the values $\{\eta_D^k(\mu_i)\}_{i=1}^{N_1}$ are independent and belong to a bounded range. Therefore, Lyapunov/Lindeberg version of the Central Limit Theorem [5, Chapter 27] can be used to deduce the approximate normality of the sample mean when the sample size N_1 is big enough. The same argument applies to the second sample $\{\eta_D^k(\nu_i)\}_{i=1}^{N_2}$, validating the use of the coordinate-wise t -test.

We apply the Behrens-Fisher-Welch t -test (without assuming equality of variances) to each coordinate of the η_D -embedding and obtain the corresponding p -values $p_k, k = 1, 2, \dots, D$. To obtain an overall p -value for the global hypothesis test of equality of means we rely on a p -value combination approach that is robust to the dependencies between the coordinates of the embedding. The harmonic mean p -value combination [15, 35] and Cauchy combination test [24] work well in this setting.

The harmonic mean p -value combination approach computes an overall p -value via the formula

$$p^H = H \left(\frac{D}{\frac{1}{p_1} + \frac{1}{p_2} + \dots + \frac{1}{p_D}} \right), \quad (2.6)$$

whereas the Cauchy combination test gives the overall p -value as

$$p^C = \frac{1}{\pi} \cot^{-1} \left(\frac{\cot \pi p_1 + \cot \pi p_2 + \dots + \cot \pi p_D}{D} \right). \quad (2.7)$$

The function H in Eq. (2.6) has a known form described in [35]. As pointed out in [31], these two methods behave very similarly for small p -values. However, we found that the Cauchy approach encounters problems when any of the p -values is very close to 1 due to the singularity of the cotangent function. This is why for our particular problem we recommend using the harmonic mean approach in real data applications.

These p -value combination methods exhibit excellent performance in practice in terms of controlling the test size, yet they have approximate nature and being introduced recently they have not gained widespread trust. This is why to guarantee explicit control for test size, [31] introduces an adjustment approach which is essentially equivalent to using the combined p -value as a test statistic and computing its null distribution via resampling. Namely, if the observed combined p -value is p^{comb} , then we generate B samples of the combined p -values, $\{p_b^{\text{comb}}\}_{b=1}^B$, from the null distribution by randomly shuffling the histograms across the groups. The adjusted p -value is then computed using the formula $p^{\text{comb adj}} = (|\{b : p_b^{\text{comb}} \leq p^{\text{comb}}\}| + 1)/(B + 1)$. The important difference between our approach and the permutation testing procedure that would use Eq. (2.4) as a test statistic is that we combine the evidence from each coordinate individually in contrast to taking the overall distance as the gross evidence against the null.

As mentioned above the granularity of the p -values after adjustment can be too coarse in multiple comparison settings. This is one reason to avoid adjustment; to decide whether adjustment is required following approach can be taken. Draw B samples as above from the null and compute the rejection rates for the p -value combination approach to verify whether they match the nominal rates. If these rates approximately match or fall to the conservative side, one should feel safe to use the un-adjusted combination p -values. For the experiments in this paper we found that p -value adjustment is not needed.

2.3 Histograms over Finite Intervals in \mathbb{R}

To exemplify our hypothesis testing framework we first provide a detailed treatment for histograms over finite intervals on the real line. This is a key building block for our general testing procedure. We assume without loss of generality that the underlying domain is an interval of the form $\mathcal{X} = [0, T]$. As the probability distance we use the 2-Wasserstein distance, $\mathcal{D} = \mathcal{W}_2$. We will first review the Hilbert property of \mathcal{W}_2 and then provide the details of the hypothesis test.

Given a probability measure $\mu \in \text{Prob}([0, T])$, let F_μ be its cumulative distribution function: $F_\mu(x) = \mu([0, x]) = \int_0^x d\mu$. The generalized inverse of CDF is defined by $F_\mu^{-1}(s) := \inf\{x \in [0, T] : F_\mu(x) > s\}$. The square of 2-Wasserstein distance has a rather simple expression in terms of the inverse CDF [28]:

$$\mathcal{W}_2^2(\mu, \nu) = \int_0^1 (F_\mu^{-1}(s) - F_\nu^{-1}(s))^2 ds.$$

This formula immediately establishes the Hilbertianity of \mathcal{W}_2 through the map $\eta : \text{Prob}([0, T]) \rightarrow L^2([0, T])$ defined by $\eta(\mu) = F_\mu^{-1}$. Using this explicit form of the mapping, the formula for \mathbb{T} from Eq. (2.4) can be written as

$$\mathbb{T} = \int_0^1 \left(\frac{1}{N_1} \sum_{i=1}^{N_1} F_{\mu_i}^{-1}(s) - \frac{1}{N_2} \sum_{i=1}^{N_2} F_{\nu_i}^{-1}(s) \right)^2 ds.$$

In practice, when working with histograms, we discretize the integral above using the Riemann sum: higher-order quadrature schemes are not warranted given the jumpy behavior of the integrand. This process can be equivalently seen through the lens of approximating the mapping η . For a selection of equidistant $s_k = \frac{k-1}{D}$, $k = 1, \dots, D$, define the approximate embedding η_D of a probability measure μ into \mathbb{R}^D as:

$$\eta_D : \mu \rightarrow \frac{1}{\sqrt{D}} [F_\mu^{-1}(s_1), F_\mu^{-1}(s_2), \dots, F_\mu^{-1}(s_D)]. \quad (2.8)$$

With this embedding, we have $\mathcal{W}_2(\mu, \nu) \approx \|\eta_D(\mu) - \eta_D(\nu)\|$, where the quality of approximation depends on the embedding dimension D .

We represent the histograms by a discrete measure of the form $\mu = \sum w_a \delta_{x_a}$ with the histogram bin centers $x_a \in [0, T]$ and weights w_a satisfying $\sum w_a = 1$, where $a = 1, 2, \dots, A$. Note that it is not required for the histograms in the collections to be supported at the same bin locations. For a given histogram, let $\{x_{(a)}, w_{(a)}\}_{a=1}^A$ be the locations sorted from smallest to largest and their corresponding weights; since the bin locations are unique there will not be any ties. The inverse CDF is computed via $F_\mu^{-1}(s) := \min\{x_{(a)} : \sum_{b \leq a} w_{(b)} > s\}$.

Using the explicit form of η_D -embedding we can now carry out the tests proposed in Section 2.2. These tests are rather intuitive, as the values of the inverse CDF in η_D -embedding correspond to the quantiles of the distribution at hand. As a result, the per-coordinate t -tests look for mean differences in s_k -th quantile of the histogram collections for each value of $s_k, k = 1, \dots, D$; the resulting p -values get combined to give the overall p -value for the global test.

3 Intrinsic Sliced 2-Wasserstein Distance

We now extend the testing methodology in Section 2.3 to cover the case of the manifold and graph domains, whose importance was discussed in the introduction. While the 2-Wasserstein distance can be straightforwardly defined in these settings, the Hilbertian property of the 2-Wasserstein distance does not carry over. For example, [28] provides a proof that \mathcal{W}_2 is not Hilbertian in \mathbb{R}^d as soon as $d > 1$. Our goal in this section is to introduce a Hilbertian version of the 2-Wasserstein distance on manifolds that inherits the desirable properties of the original \mathcal{W}_2 . The approach is inspired by the success of the sliced Wasserstein distances [21]. While the original slicing has been extended to more complex settings [20], it is based on extrinsic constructs and can fail to capture the intrinsic properties of the manifold. We propose a new approach to slicing that is intrinsic to the manifold; we call this *intrinsic slicing*.

Before proceeding, we review several notions that will be needed for our construction. To focus our discussion we concentrate on the manifold case, as the graph case is simpler; in fact, some of the theorems in the next subsections are trivial due to the finite nature of graphs. Let λ_ℓ and ϕ_ℓ with $\ell = 0, 1, \dots$ be the eigenvalues and eigenfunctions of the Laplace-Beltrami operator on \mathcal{X} with Neumann boundary conditions. The eigenfunctions are assumed to be orthonormal with respect to the uniform measure on \mathcal{X} ; also $\phi_0 = \text{const}$ and $\lambda_0 = 0$. One can define the spectral kernel $k(x, y) = \sum_\ell \alpha(\lambda_\ell) \phi_\ell(x) \phi_\ell(y)$ and the corresponding spectral distance on the manifold $d(x, y) = k(x, x) + k(y, y) - 2k(x, y) = \sum \alpha(\lambda_\ell) (\phi_\ell(x) - \phi_\ell(y))^2$, where $\alpha : \mathbb{R}_{\geq 0} \rightarrow \mathbb{R}_{\geq 0}$ is a function that controls contribution from each spectral band. By setting $\alpha(\lambda) = e^{-t\lambda}$ for some $t > 0$, we get the well-known heat/diffusion kernel and the corresponding diffusion distance [10]. Another important case is $\alpha(\lambda) = 1/\lambda^2$ if $\lambda > 0$ and $\alpha(0) = 0$, which gives the biharmonic kernel and distance [23]. Biharmonic distance has been shown to work well on low-dimensional manifolds and does not require setting any parameters. Note that in both of these constructions $\alpha(\cdot)$ is a decreasing function, which allows the smoother low-frequency (i.e. smaller λ_ℓ) eigenfunctions to contribute more.

3.1 Intrinsic Sliced Distance

A real-valued function $\phi : \mathcal{X} \rightarrow \mathbb{R}$ can be used to map the manifold \mathcal{X} onto the real line. Any probability measure $\mu \in \mathcal{P}(\mathcal{X})$ can likewise be projected onto the real line using the pushforward of ϕ , which we denote by $\phi\#\mu = \mu \circ \phi^{-1} \in \mathcal{P}(\mathbb{R})$. Based on this insight, we define intrinsic slicing as follows.

Definition 2. Given a function $\alpha : \mathbb{R}_{\geq 0} \rightarrow \mathbb{R}_{\geq 0}$ and a probability distance $\mathcal{D}(\cdot, \cdot)$ on $\mathcal{P}(\mathbb{R})$, we define the intrinsic sliced distance $IS\mathcal{D}(\cdot, \cdot)$ on $\mathcal{P}(\mathcal{X})$ by

$$IS\mathcal{D}^2(\mu, \nu) = \sum_{\ell} \alpha(\lambda_{\ell}) \mathcal{D}^2(\phi_{\ell} \# \mu, \phi_{\ell} \# \nu).$$

The choice of the Laplacian eigenfunctions in the definition can be justified by a number of their properties. Eigenfunctions are intrinsic quantities of a manifold and are ordered by smoothness. Thus, they allow capturing the intrinsic connectivity of the underlying domain. Furthermore, due to the orthogonality of eigenfunctions, the corresponding pushforwards are able to capture complementary aspects of the distribution.

While the definition is general, our focus in this paper is on the case when $\mathcal{D} = \mathcal{W}_2$. To avoid confusion we always use \mathcal{W}_2 to denote the 2-Wasserstein distance on $\mathcal{P}(\mathbb{R})$. We call the resulting distance *Intrinsic Sliced 2-Wasserstein Distance*, and denote it by $IS\mathcal{W}_2$. First, we discuss the convergence of the infinite sum in the definition.

Proposition 2. *If \mathcal{X} is a smooth compact n -dimensional manifold and $\sum_{\ell} \lambda_{\ell}^{(n-1)/2} \alpha(\lambda_{\ell}) < \infty$, then $IS\mathcal{W}_2$ is well-defined.*

Proof. We use Hörmander's bound on the supremum norm of the eigenfunctions:

$$\|\phi_{\ell}\|_{\infty} \leq c \lambda_{\ell}^{(n-1)/4} \|\phi_{\ell}\|_2,$$

for some constant c that depends on the manifold. By orthonormality of the eigenfunctions we have $\forall \ell, \|\phi_{\ell}\|_2 = 1$. Next, note that $\mathcal{W}_2(\phi_{\ell} \# \mu, \phi_{\ell} \# \nu) \leq 2 \|\phi_{\ell}\|_{\infty}$ as the maximum distance that the mass would be transported in any transportation plan involving pushforwards via ϕ_{ℓ} is upper bounded by $2 \|\phi_{\ell}\|_{\infty}$. As a result, every term in the series defining $IS\mathcal{W}_2$ can be upper-bounded by the terms of the following series:

$$\sum_{\ell} 4 \|\phi_{\ell}\|_{\infty}^2 \alpha(\lambda_{\ell}) \leq \sum_{\ell} 4c^2 \lambda_{\ell}^{(n-1)/2} \alpha(\lambda_{\ell}) \propto \sum_{\ell} \lambda_{\ell}^{(n-1)/2} \alpha(\lambda_{\ell}),$$

which proves the claim by the direct comparison test for convergence of series. \square

When Weyl law applies, we have that $\lambda_{\ell} = \Theta(\ell^{2/n})$, which allows us to use the condition $\sum_{\ell} \ell^{(n-1)/n} \alpha(\lambda_{\ell}) < \infty$. For the diffusion kernel/distance choice of $\alpha(\lambda) = e^{-t\lambda}$ the series always converges independently of the manifold dimension. For biharmonic choice of $\alpha(\lambda) = 1/\lambda^2$, the sufficient condition is the convergence of $\sum_{\ell} \ell^{(n-1)/n} / \lambda_{\ell}^2 \sim \sum_{\ell} \ell^{(n-1)/n} / (\ell^{2/n})^2 = \sum_{\ell} \ell^{(n-5)/n}$, where we applied Weyl's asymptotic again. As a result, the biharmonic choice of α is guaranteed to provide a well-defined $IS\mathcal{W}_2$ for 1 and 2-dimensional manifolds. Notice, however, that the Hörmander's bound can be rather lax in some of the settings that are practically relevant, such as the product spaces of lines and circles, where all of the eigenfunctions are bounded by a constant as can be seen from Table 1.

3.2 Properties of $IS\mathcal{D}$

We now prove a number of properties of intrinsic sliced distances that demonstrate their usefulness for our testing problem.

Proposition 3. *If \mathcal{D} is a Hilbertian probability distance such that $IS\mathcal{D}$ is well-defined, then*

- (i) *$IS\mathcal{D}$ is Hilbertian, and*
- (ii) *$IS\mathcal{D}$ satisfies the following metric properties: non-negativity, symmetry, the triangle inequality, and $IS\mathcal{D}(\mu, \mu) = 0$.*

Proof. By Hilbertian property, there exists a Hilbert space \mathcal{H} such that $\mathcal{D}(\rho_1, \rho_2) = \|\eta(\rho_1) - \eta(\rho_2)\|_{\mathcal{H}}$ for all $\rho_1, \rho_2 \in \mathcal{P}(\mathbb{R})$. Plugging this into the definition of the intrinsic sliced distance we see that $ISD(\mu, \nu) = \|\eta^*(\mu) - \eta^*(\nu)\|_{\mathcal{H}^*}$, where $\mathcal{H}^* = \oplus_{\ell} \mathcal{H}$ and the ℓ -th component of $\eta^*(\mu)$ is $\sqrt{\alpha(\lambda_{\ell})} \eta(\phi_{\ell} \# \mu) \in \mathcal{H}$. The second part of the proposition directly follows from the Hilbert property. \square

Since \mathcal{W}_2 is Hilbertian on $\mathcal{P}(\mathbb{R})$, the application of Proposition 3 yields that ISW_2 is also Hilbertian, making it possible to use ISW_2 for our hypothesis testing framework laid out in Section 2.

The following result shows that ISW_2 inherits an important property of the Wasserstein distances, namely that the distance between two Dirac delta measures equals to a specific ground distance between their locations.

Proposition 4. *When $\mu = \delta_x(\cdot)$ and $\nu = \delta_y(\cdot)$ for two points $x, y \in \mathcal{X}$, we have $ISW_2(\mu, \nu) = d(x, y)$, where $d(\cdot, \cdot)$ is the spectral distance corresponding to the choice of $\alpha(\cdot)$.*

Proof. We have $\phi_{\ell} \# \delta_x = \delta_{\phi_{\ell}(x)}$ and similarly for y . Now $\mathcal{W}_2^2(\phi_{\ell} \# \mu, \phi_{\ell} \# \nu) = \mathcal{W}_2^2(\delta_{\phi_{\ell}(x)}, \delta_{\phi_{\ell}(y)}) = (\phi_{\ell}(x) - \phi_{\ell}(y))^2$. This last equality follows from the fact that the 2-Wasserstein on real line between delta measures is equal to the distance between the two points. Then scaling and adding up gives exactly the kernel distance $d(x, y)$ between the two points. \square

Next we consider a rather simple choice of distance \mathcal{D} on $\mathcal{P}(\mathbb{R})$, namely the absolute mean difference and show that the corresponding intrinsic sliced distance is the MMD [17].

Proposition 5. *Let $\mathcal{D}(\rho_1, \rho_2) = |\mathbb{E}_{x \sim \rho_1}[x] - \mathbb{E}_{y \sim \rho_2}[y]|$ for $\rho_1, \rho_2 \in \mathcal{P}(\mathbb{R})$, then the corresponding intrinsic sliced distance is equivalent to the MMD with the spectral kernel $k(\cdot, \cdot)$.*

Proof. We can rewrite the definition as follows:

$$\begin{aligned} ISD^2(\mu, \nu) &= \sum_{\ell} \alpha(\lambda_{\ell}) (\mathbb{E}_{x \sim \phi_{\ell} \# \mu}[x] - \mathbb{E}_{y \sim \phi_{\ell} \# \nu}[y])^2 = \sum_{\ell} \alpha(\lambda_{\ell}) (\mathbb{E}_{x \sim \mu}[\phi_{\ell}(x)] - \mathbb{E}_{y \sim \nu}[\phi_{\ell}(y)])^2 \\ &= \sum_{\ell} \alpha(\lambda_{\ell}) (\mathbb{E}_{x, x' \sim \mu}[\phi_{\ell}(x)\phi_{\ell}(x')] + \mathbb{E}_{y, y' \sim \nu}[\phi_{\ell}(y)\phi_{\ell}(y')] - 2\mathbb{E}_{x \sim \mu, y \sim \nu}[\phi_{\ell}(x)\phi_{\ell}(y)]) \\ &= \mathbb{E}_{x, x' \sim \mu}[\sum_{\ell} \alpha(\lambda_{\ell}) \phi_{\ell}(x)\phi_{\ell}(x')] + \mathbb{E}_{y, y' \sim \nu}[\sum_{\ell} \alpha(\lambda_{\ell}) \phi_{\ell}(y)\phi_{\ell}(y')] \\ &\quad - 2\mathbb{E}_{x \sim \mu, y \sim \nu}[\sum_{\ell} \alpha(\lambda_{\ell}) \phi_{\ell}(x)\phi_{\ell}(y)] \\ &= \mathbb{E}_{x, x' \sim \mu}[k(x, x')] + \mathbb{E}_{y, y' \sim \nu}[k(y, y')] - 2\mathbb{E}_{x \sim \mu, y \sim \nu}[k(x, y)], \end{aligned}$$

where we used the spectral kernel $k(x, y) = \sum_{\ell} \alpha(\lambda_{\ell}) \phi_{\ell}(x)\phi_{\ell}(y)$. The last expression coincides with MMD based on kernel $k(\cdot, \cdot)$; see Lemma 6 in [17]. \square

When $k(x, y)$ is the heat kernel, this is very much like the MMD with the Gaussian kernel, with the parameter t in $\alpha(\lambda) = e^{-t\lambda}$ controlling the kernel width. Not only the heat kernel in \mathbb{R}^d coincides with the Gaussian kernel, but also on general manifolds Varadhan's formula gives an asymptotic equivalence for small values of t .

An interesting insight that can be derived from the above result is that ISW_2 is in a sense a "stronger" distance than MMD that uses the corresponding spectral kernel. The ISW_2 compares the quantiles of the pushforward distributions, whereas MMD compares their expectations only. We formalize this notion in the following proposition, which also provides a theoretical reason for preferring ISW_2 for hypothesis testing.

Proposition 6. $MMD(\mu, \nu) \leq ISW_2(\mu, \nu)$ when the same $\alpha(\cdot)$ is used in both constructions.

Proof. This follows directly from the fact that for $\rho_1, \rho_2 \in \mathcal{P}(\mathbb{R})$ the inequality $|\mathbb{E}_{x \sim \rho_1}[x] - \mathbb{E}_{y \sim \rho_2}[y]| \leq \mathcal{W}_2(\rho_1, \rho_2)$ holds. \square

Now we can prove that ISW_2 is a true metric.

Theorem 1. If $\alpha(\lambda) > 0$ for all $\lambda > 0$, then ISW_2 is a metric on $\mathcal{P}(\mathcal{X})$.

Proof. In the light of the Proposition 3 it remains only to prove that $ISW_2(\mu, \nu) = 0$ implies $\mu = \nu$. According to the previous proposition, $ISW_2(\mu, \nu) = 0$ yields $MMD(\mu, \nu) = 0$. The assumption that $\alpha(\lambda) > 0$ for all $\lambda > 0$ implies that the spectral kernel $k(\cdot, \cdot)$ corresponding to $\alpha(\cdot)$ is universal [25]. Universality implies the characteristic property [17], which in turn means that $MMD(\mu, \nu) = 0$ is equivalent to $\mu = \nu$, proving the claim. \square

We remind that 2-Wasserstein distance can be defined directly on $\mathcal{P}(\mathcal{X})$ using the geodesic distance as the ground metric; to avoid confusion we denote this as $\mathcal{W}_2^{\mathcal{X}}$. Using Lipschitz properties of eigenfunctions we now prove the following:

Proposition 7. There exists a constant c depending only on \mathcal{X} such that for all $\mu, \nu \in \mathcal{P}(\mathcal{X})$ the inequality $ISW_2(\mu, \nu) \leq c\mathcal{W}_2^{\mathcal{X}}(\mu, \nu)\sqrt{\sum_{\ell} \lambda_{\ell}^{(n+3)/2} \alpha(\lambda_{\ell})}$ holds; here, n is the dimension of \mathcal{X} .

Proof. The Neumann eigenfunctions on compact manifolds satisfy the inequality $\|\nabla \phi_{\ell}\|_{\infty} \leq c_1 \lambda_{\ell} \|\phi_{\ell}\|_{\infty}$, see [18]. Applying the bound used in the proof of convergence, $\|\phi_{\ell}\|_{\infty} \leq c_2 \lambda_{\ell}^{(n-1)/4}$, we get that ϕ_{ℓ} is Lipschitz with respect to the geodesic distance on \mathcal{X} with the Lipschitz constant bounded by $c\lambda_{\ell} \lambda_{\ell}^{(n-1)/4} = c\lambda_{\ell}^{(n+3)/4}$.

Consider the optimal coupling between μ and ν whose cost equals to $\mathcal{W}_2^{\mathcal{X}}(\mu, \nu)$. Note that this coupling straightforwardly provides a coupling between the pushforwards $\phi_{\ell} \# \mu$ and $\phi_{\ell} \# \nu$. Using the Lipschitz property of eigenfunctions, we see that the cost of the pushforward coupling is smaller than $c\lambda_{\ell}^{(n+3)/4} \mathcal{W}_2^{\mathcal{X}}(\mu, \nu)$. Since any such coupling provides an upper bound on $\mathcal{W}_2(\phi_{\ell} \# \mu, \phi_{\ell} \# \nu)$, we have $\mathcal{W}_2(\phi_{\ell} \# \mu, \phi_{\ell} \# \nu) \leq c\lambda_{\ell}^{(n+3)/4} \mathcal{W}_2^{\mathcal{X}}(\mu, \nu)$. Plugging this into the formula for ISW_2 we get the claimed bound. \square

Our final result shows that the quantity \mathbb{T} defined via ISW_2 enjoys robustness with respect to small perturbations of the measures in the collection.

Proposition 8. Let $\{\mu_i\}_{i=1}^N$ and $\{\nu_i\}_{i=1}^N$ be two collections of probability measures on $\mathcal{P}(\mathcal{X})$, such that $\forall i, \mathcal{W}_2^{\mathcal{X}}(\mu_i, \nu_i) \leq \epsilon$, then $\mathbb{T}(\{\mu_i\}_{i=1}^N, \{\nu_i\}_{i=1}^N) \leq C^2 \epsilon^2$. Here $C = c\sqrt{\sum_{\ell} \lambda_{\ell}^{(n+3)/2} \alpha(\lambda_{\ell})}$ from previous proposition and is assumed to be finite.

Proof. We have

$$\begin{aligned} \mathbb{T}(\{\mu_i\}_{i=1}^N, \{\nu_i\}_{i=1}^N) &= \left\| \frac{1}{N} \sum_{i=1}^N \eta(\mu_i) - \frac{1}{N} \sum_{i=1}^N \eta(\nu_i) \right\|^2 = \left\| \frac{1}{N} \sum_{i=1}^N (\eta(\mu_i) - \eta(\nu_i)) \right\|^2 \\ &\leq \frac{1}{N} \sum_{i=1}^N \|\eta(\mu_i) - \eta(\nu_i)\|^2 = \frac{1}{N} \sum_{i=1}^N ISW_2^2(\mu_i, \nu_i) \leq \frac{1}{N} \sum_{i=1}^N (C\mathcal{W}_2^{\mathcal{X}}(\mu_i, \nu_i))^2 \\ &\leq \frac{1}{N} N(C\epsilon)^2 = C^2 \epsilon^2. \end{aligned}$$

\square

The above bound in terms of $\mathcal{W}_2^{\mathcal{X}}$ implies that if the distributions in a collection undergo horizontal shifts (i.e. movement along the domain) that are small as measured by the geodesic distance (captured via $\mathcal{W}_2^{\mathcal{X}}$), then the quantity \mathbb{T} cannot change drastically.

4 Tests for Histograms on Manifolds and Graphs

In this section we go over the implementation details of conducting tests on histograms defined over manifold and graph domains. The main requirement for our testing procedure is the Hilbertian property, which is satisfied by ISW_2 as shown in Proposition 3. Denoting by η the corresponding Hilbert embedding, our goal is to obtain its finite dimensional approximation of the form $\eta_D : \mathcal{P}(\mathcal{X}) \rightarrow \mathbb{R}^D$.

By inspecting the proof of Proposition 3 we see that η is composed of individual Hilbert embeddings (i.e. via the inverse CDF) of \mathcal{W}_2 on \mathbb{R} , one per term of the series defining the ISW_2 . To obtain the finite dimensional approximate embedding, we truncate the series for ISW_2 , namely we use a finite number of eigenfunctions for pushforward: $\phi_\ell, \ell = 1, \dots, L$, where ϕ_0 is dropped since it is a constant. Using the approximate embedding from Eq. (2.8) for \mathcal{W}_2 on $\mathcal{P}(\mathbb{R})$, we obtain the following as the components of η_D corresponding to the eigenfunction ϕ_ℓ :

$$(\eta_D)_\ell : \mu \rightarrow \sqrt{\frac{\alpha(\lambda_\ell)}{D'}} [F_{\phi_\ell \# \mu}^{-1}(s_1), F_{\phi_\ell \# \mu}^{-1}(s_2), \dots, F_{\phi_\ell \# \mu}^{-1}(s_{D'})],$$

where $s_k = \frac{k-1}{D'}, k = 1, \dots, D'$. Note that the dimensionality of the overall approximate embedding is $D = LD'$.

As before, we represent the histograms by a discrete measure of the form $\sum w_a \delta_{x_a}$ with the histogram bin centers $x_a \in \mathcal{X}$ and weights w_a satisfying $\sum w_a = 1$, where $a = 1, 2, \dots, A$. The pushforward $\phi_\ell \# \mu$ gives a histogram on the real line defined by $\sum w_a \delta_{\phi_\ell(x_a)}$. Note that while x_a are distinct, their images under ϕ_ℓ do not have to be distinct, so one re-aggregates the weights to obtain $\sum_{a \in S} w'_a \delta_{\phi_\ell(x_a)}$, where S is a subset of $1, 2, \dots, A$ and w'_a are the new weights. It is now straightforward to compute the inverse CDF for each of the values s_k and build the η_D -embedding.

Using the explicit form of η_D -embedding we can carry out the p -value combination test as described in Section 2. Interestingly, in the p -value combination test the scaling $\sqrt{\alpha(\lambda_\ell)}$ cancels out when performing the coordinate-wise t -tests. However, these scalings can potentially be used in the p -value combination approaches to modify the contribution of each coordinate. If one would like to run the permutation test using the quantity \mathbb{T} from Eq. (2.4) as the test statistic, then the choice of the function $\alpha(\cdot)$ matters. When working on manifolds of low dimension, either 1 or 2, the choice of $\alpha(\cdot)$ that corresponds to the biharmonic distance is convenient. While the diffusion distance provides a general choice that works on manifolds of any dimension, the biharmonic distance does not have any parameters to tune and was shown to provide an excellent alternative to the geodesic distance in low-dimensional settings [23]. The importance of relying on a well-behaved spectral distance was highlighted in Proposition 4.

The proposed approach can be carried out on very general manifolds, represented by graphs or point clouds in practice. In such general settings the spectral decomposition of the Laplace-Beltrami operator has to be computed numerically. For applications that involve simple manifolds, the eigenvalues and eigenfunctions can be computed analytically. For completeness we list them in Table 1. Note that we benefit from the fact that the eigen-decomposition for product spaces can be derived from the eigen-decompositions of the components.

Remark 3. A major benefit of the p -value combination approach is that the resulting test is *interpretable*. Since the coordinates of the η_D -embeddings correspond to quantiles in the pushforwards,

\mathcal{X}	Eigenvalues	Eigenfunctions
$[0, T]$	$(\frac{\pi\ell}{T})^2$	$\sqrt{\frac{2}{T}} \cos \frac{\pi\ell x}{T}$
$S^1(T) = [0, T] \text{ mod } T$	$(\frac{2\pi\ell}{T})^2$	$\sqrt{\frac{2}{T}} [\cos / \sin] \frac{2\pi\ell x}{T}$
$[0, T_1] \times [0, T_2]$	$(\frac{\pi\ell_1}{T_1})^2 + (\frac{\pi\ell_2}{T_2})^2$	$\sqrt{\frac{4}{T_1 T_2}} \cos \frac{\pi\ell_1 x}{T_1} \cos \frac{\pi\ell_2 x}{T_2}$
$S^1(T_1) \times [0, T_2]$	$(\frac{2\pi\ell_1}{T_1})^2 + (\frac{\pi\ell_2}{T_2})^2$	$\sqrt{\frac{4}{T_1 T_2}} [\cos / \sin] \frac{2\pi\ell_1 x}{T_1} \cos \frac{\pi\ell_2 x}{T_2}$
$S^1(T_1) \times S^1(T_2)$	$(\frac{2\pi\ell_1}{T_1})^2 + (\frac{2\pi\ell_2}{T_2})^2$	$\sqrt{\frac{4}{T_1 T_2}} [\cos / \sin] \frac{2\pi\ell_1 x}{T_1} [\cos / \sin] \frac{\pi\ell_2 x}{T_2}$
S^2		Spherical harmonics [6]
Graphs/Data Clouds/Meshes	Eigen-decomposition of the Laplacian matrix	

Table 1: Eigenvalues and eigenfunctions of the Laplace-Beltrami operator with Neumann boundary conditions for simple manifolds. We exclude zero eigenvalue and the corresponding constant eigenvector; thus, all indices ℓ, ℓ_1, ℓ_2 run over positive integers. The notation $[\cos / \sin]$ means picking either the cosine or sine function- *both choices must be used, giving multiple eigenfunctions*.

one can find and study the coordinates that exhibit the most difference to obtain further insights about the dissimilarity between the groups.

5 Experiments

5.1 Simulated Data

We evaluate the proposed testing procedure using numerical experiments in several data settings. For each setting, we compare nominal sizes and powers for a number of alternate hypotheses obtained using our method with several existing methods. We evaluate all methods using empirical power at different degrees of departure from the null hypothesis, calculated by averaging the proportion of rejections at level 0.05 over 1000 independent datasets with samples divided into two groups inside each dataset. To ensure the tests are well-calibrated, we also calculate nominal sizes assuming the two sample groups are drawn from the same random process.

Distributions over finite intervals Samples obtained from functions that take values on finite intervals can be transformed to histograms by simple location shifts [19]. To obtain our base measures μ_i, ν_i , we use the experimental setting of [36] to generate bin probabilities as (shifted and normalized) values of the function below at $m = 30$ fixed design points $t_j = j/(m + 1), j = \{1, 2, \dots, m\}$:

$$\begin{aligned}
 f(t) &= \mu(t) + \alpha(t), \\
 \mu(t) &= 1.2 + 2.3 \cos(2\pi t) + 4.2 \sin(2\pi t), \\
 \alpha(t) &= \epsilon_0 + \sqrt{2}\epsilon_1 \cos(2\pi t) + \sqrt{3}\epsilon_2 \sin(2\pi t),
 \end{aligned}$$

where $\epsilon_0, \epsilon_1, \epsilon_2 \sim N(0, 1)$, and $t \in \{t_1, \dots, t_m\}$. We generate $N_1 = 60$ samples for the first group as independent realizations of the above random process: $\mu_i(\cdot) \equiv f(\cdot)$. For the second group, we generate $N_2 = 40$ samples from a shifted process: $\nu_i(\cdot) \equiv f(\cdot) + \delta(\cdot)$, where $\delta(t) = \delta$ for all $t \in \{t_1, \dots, t_m\}$ is a constant amount of location shift. After generating all measures for samples

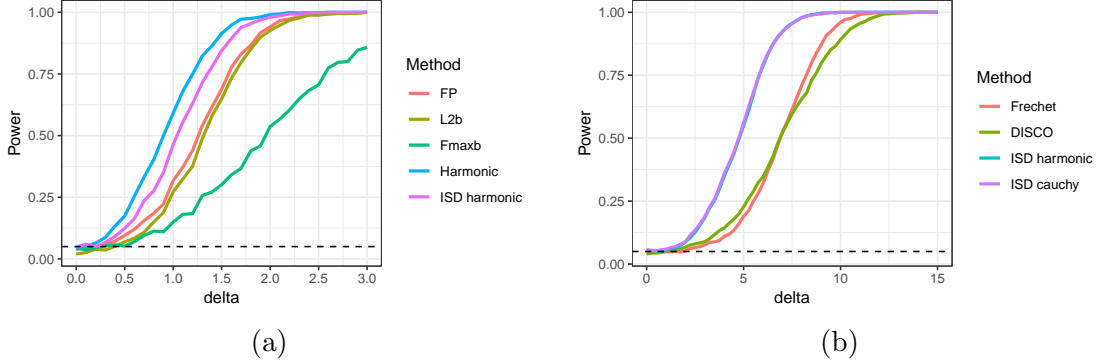


Figure 2: Empirical powers across different alternate hypotheses for (a) finite interval data and (b) circular data numerical experiments. Dotted lines indicate the level of all tests (0.05).

in the two groups, we shift all function values by the minimum negative magnitude across both groups and all values of t to make them non-negative. Finally, as the m -length vector of bin counts for a sample, we generate a random vector from the Multinomial distribution with 1000 trials, m outcomes and the outcome probabilities proportional to the shifted functional observations corresponding to that sample. To quantify the effect of different degrees of departure from the null hypothesis, we consider a range of values for $\delta \in [0, 3]$, so that mean rejection proportions for $\delta = 0$ at level 0.05 indicates the nominal size of a test, and that for $\delta = 3$ gives empirical power.

We compared our finite interval approach from Section 2.2 with embedding dimension $D = 20$ against the 11 functional ANOVA tests in the R package `fdANOVA`. While our proposal outperformed all the other tests across all values of δ , for brevity we only report results for 3 of the other methods that use different methodological approaches (see Table 5 in Appendix for the complete set of results). These 3 methods include the permutation test based on basis function representation (FP in Figure 2a) [16], the sum-type ℓ_2 norm-based bootstrap test (L2b) [37], and the max-type bootstrap test of [38] that uses the maximum of coordinate-wise F statistic (Fmaxb). For clarity we report in Figure 2a results for the harmonic p -value combinations, which performed better among the two. All methods maintain nominal size for $\delta = 0$.

Curiously, we can apply the intrinsic slicing construction to the finite interval case. This gives rise to another test and we include it in the above comparisons in order to gain insight about the effect of slicing on the testing power. To implement our ISW_2 -based testing procedure, we use $L = 4$ eigenfunctions and $D' = 5$ for the inverse CDF transformation; this gives an overall embedding of dimension $D = 20$, same as for the unsliced version above. Analytical expressions for the eigenfunctions and eigenvalues required for our slicing construction are given in the first row of Table 1. We display the results from harmonic combination in Figure 2a; the Cauchy p -value combination results are available in the appendix. The sliced version is more powerful than all the other tests, except it performs slightly worse than the unsliced version (“ISD harmonic” and “Harmonic” respectively). The latter is expected: slicing is not required for the finite interval case as our approach from Section 2.2 can handle it directly.

Circular distributions Analysis of circular datasets is important in a number of diverse application areas, such as ecology, medical sciences and psychology [11]. To evaluate our proposal in this data setting, we consider as our samples μ_i, ν_i von Mises distributions with randomly chosen parameters. For an angle x (measured in radians), the von Mises probability density function is given by

$$f(x|\mu, \kappa) = \frac{e^{\kappa \cos(x-\mu)}}{2\pi I_0(\kappa)},$$

where $I_0(\kappa)$ is the modified Bessel function of order 0. In our experiments, we use $\mu \equiv \mu_i \sim N(0, 0.1^2)$ and $\nu \equiv \nu_i \sim N(\delta, 0.1^2)$ to simulate the means for samples from group 1 and 2 respectively, and fix $\kappa = 2$ across both groups. As each observation vector, we obtain 100 i.i.d. observations from these sample-specific circular distributions. Given a δ , we draw $N_1 = 60$ and $N_2 = 40$ such samples for the two groups to construct a dataset, and consider 1000 replications of this setup. Finally, we repeat the above for $\delta \in [0, 15] \times \pi/180$ (i.e. 0 to 15 degrees converted to radians).

For our method, we use the first $L = 10$ eigenfunctions, and a $D' = 20$ dimensional inverse CDF transformation to obtain high-dimensional embeddings for the sample measures. The eigenfunctions and eigenvalues over a circle needed to calculate pushforwards for are given in the second row of Table 1. Note that we use both cosine and sine transformations to calculate pushforwards of distributions on a circle, so our final embedding dimension is $10 \times 20 \times 2 = 400$. As competing methods, we consider the recently proposed bootstrap-based Fréchet ANOVA test [13] (indicated by Fréchet in Figure 2b), and the distance-component based nonparametric test by [30] (DISCO). Since these approaches cannot handle the circular geometry directly, we cut it into an interval. Similar to the previous experimental setup, we calculate empirical size for $\delta = 0$, and power across non-zero values of δ for all methods. The results are summarized in Figure 2b. All methods maintain nominal size, but both the p -value combinations obtained from coordinate-wise tests on the embedding dimensions exhibit considerably higher power across δ than the existing methods.

5.2 Real Data

NHANES data on physical activity monitoring As our first real data application, we analyze the Physical Activity Monitor (PAM) data from the 2005-2006 National Health and Nutrition Examination Survey (NHANES)¹. This contains physical activity pattern readings for a large number of people collected over 1 week period on a per-minute granularity. After basic pre-processing steps to ensure no missing entries, as well as data reliability and well-calibrated activity monitors, we use data from 6839 individuals. The data for each individual corresponds to device intensity value from the PAM for $24 \times 60 = 1440$ minutes throughout the day, for 7 days.

For each individual we can capture their activity patterns into a cylindrical histogram with time and intensity dimensions. For each observation, its time during the day is discretized into 15-minute intervals giving 96 bins for the time dimension; its intensity value (capped at 10,000) is discretized into a 100 equidistant bins. Since the time dimension is periodic, we obtain a histogram over the cylinder $S^1(T_1) \times [0, T_2)$, with $T_1 = 96, T_2 = 100$. Normalized counts can thus be considered as person-specific probability distributions; several examples are shown in Figure 3. Note that flattening the domain by cutting the cylinder will arbitrarily split activity patterns (see especially Figure 3c) and will lead to inefficiencies in capturing horizontal variability.

We will apply the proposed methodology to check if the activity patterns vary across different groups of individuals obtained as follows. We first split the overall dataset based on the individual’s age using the following inclusive ranges: 6–15, 16–25, ..., 76–85; this covers all the ages in the dataset. From each split we sample 100 males and 100 females to avoid gender imbalance driving the results. Thus, we end up with 8 age groups with 200 individuals per group. Our goal is to compare these 8 groups’ activity patterns by conducting pair-wise tests.

¹https://www.cdc.gov/Nchs/Nhanes/2005-2006/PAXRAW_D.htm

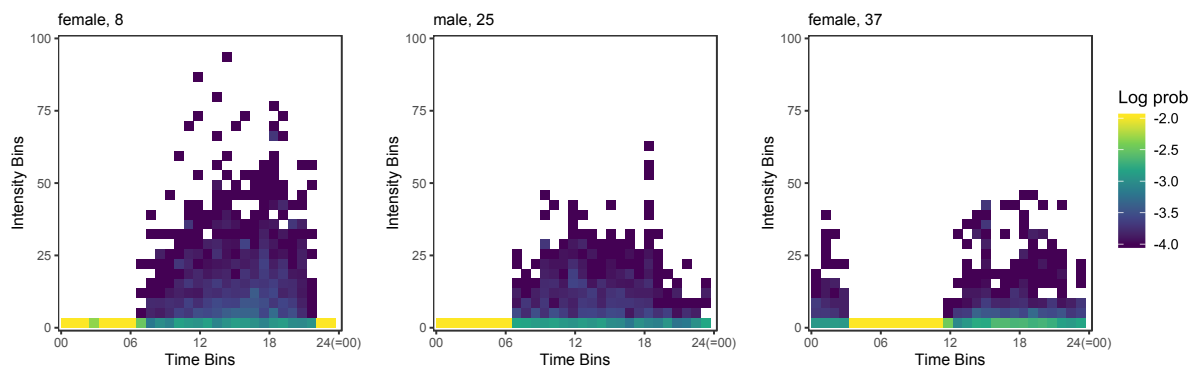


Figure 3: Activity histograms for three individuals from NHANES dataset. There are 100 bins in the intensity and 96 in the time dimension; we show hour of day on the time axis. The time dimension is periodic where 00:00 is identified with 24:00, giving rise to a cylindrical histogram domain.

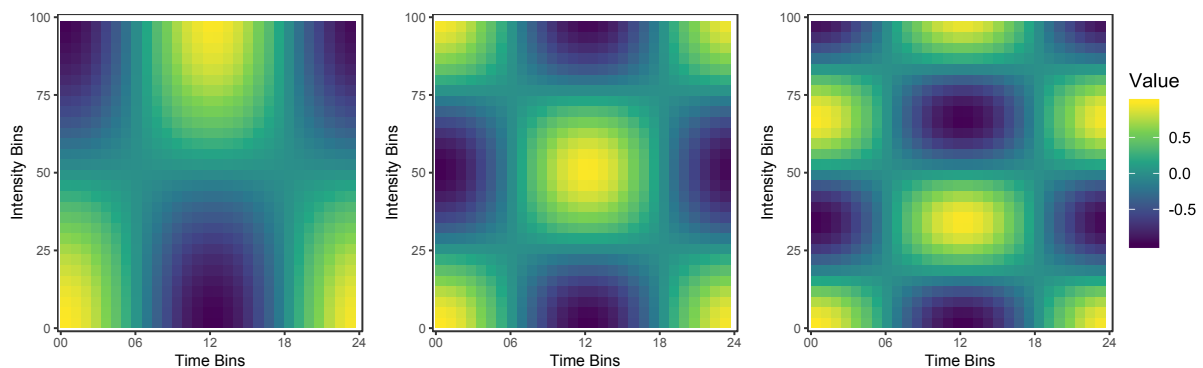


Figure 4: Three eigenfunctions for the NHANES histogram domain normalized by the maximum absolute value. Note that the eigenfunctions are periodic in the time direction (i.e. match when glued over the side cut) but not in the intensity direction, reflecting the cylindrical geometry of the underlying domain.

Age Groups	6–15	16–25	26–35	36–45	46–55	56–65	66–75	76–85
6–15		0.394	0.098	0.555	0.882	0.985	0.919	0.997
16–25	1.2e-13		0.575	0.967	0.126	0.921	0.911	0.977
26–35	3.1e-21	2.7e-04		0.459	0.197	0.996	0.919	0.565
36–45	6.1e-22	7.9e-08	0.042		0.864	0.637	0.849	0.991
46–55	8.2e-22	4.7e-05	0.011	0.343		0.841	0.165	0.554
56–65	1.3e-25	0.001	0.001	5.6e-05	0.003		0.991	0.962
66–75	3.6e-35	7.8e-12	1.5e-11	4.6e-15	1.8e-13	0.001		0.989
76–85	3.8e-46	1.4e-26	1.7e-30	8.4e-37	2.1e-35	1.3e-17	6.5e-09	

Table 2: Comparing the activity intensity of different age groups based on the NHANES dataset. Below diagonal: p -values corresponding to the actual data comparisons. Above diagonal: null p -values obtained by combining and randomly splitting the two involved groups. The entries in boldface correspond to the rejected hypotheses with the BH procedure at the FDR level of 0.1.

To perform our analysis we compute the eigenvalues and eigenfunctions as per the 4th row of Table 1. The top 3 indices along the first direction, i.e. $\ell_1 = 1, 2, 3$ and top 3 indices along the second direction, i.e. $\ell_2 = 1, 2, 3$ are used; three of the resulting eigenfunctions are shown in Figure 4. We consider a $D' = 5$ dimensional embedding for the inverse CDF transformation, hence the final embedding dimension after the slicing construction is $D = 2 \times 3 \times 3 \times 5 = 90$.

We summarize the results in Table 2, *below the diagonal*. The p -values are obtained via the harmonic mean combination approach. We run the Benjamini-Hochberg [3] procedure on the resulting p -values at the false discovery rate of 0.1, and the rejected hypotheses are indicated by the p -values in bold. Our method detects statistically significant differences between all pairs of groups, except the 36–45 and 46–55 groups. As a control experiment, we provide our method with null cases and display the p -values in Table 2, *above the diagonal*. The null cases are obtained by combining the individuals from the two comparison groups and splitting it arbitrarily (i.e. mixing the two age groups). As expected, the p -values of the control comparisons do not concentrate near zero.

Curiously, our method can be used “off-label” to conduct functional data analyses over different dimensions of the NHANES dataset. For example, one can concentrate on a single day of activity intensity data which gives a curve over the 24-hour circle. Since activity intensity is a non-negative number, these curves can be normalized so as to obtain probability distributions. Now we can use our methodology to detect pair-wise differences across groups. While this has the benefit of accounting for underlying geometry of data, it loses the absolute magnitude information due to the normalization. Clearly the appropriateness of such an analysis would depend on the goal of the exercise and the particular research question attached to that goal; our proposal provides a framework that is flexible enough to handle data of different modalities.

Chicago Crime We demonstrate the use of our methodology on histograms over graphs. In this experiment, we use the Chicago Crimes 2018 dataset² which captures incidents of crime in the City of Chicago. We base our analysis on the type of crime, the beat (geographic area subdivision used by police, see Figure 5) where the incident took place, and the date of the incident. To capture the spatial aspect of the data we build a graph with one vertex per beat; two vertices are connected by an edge if the corresponding beats share a geographic boundary. For each crime

²data.cityofchicago.org

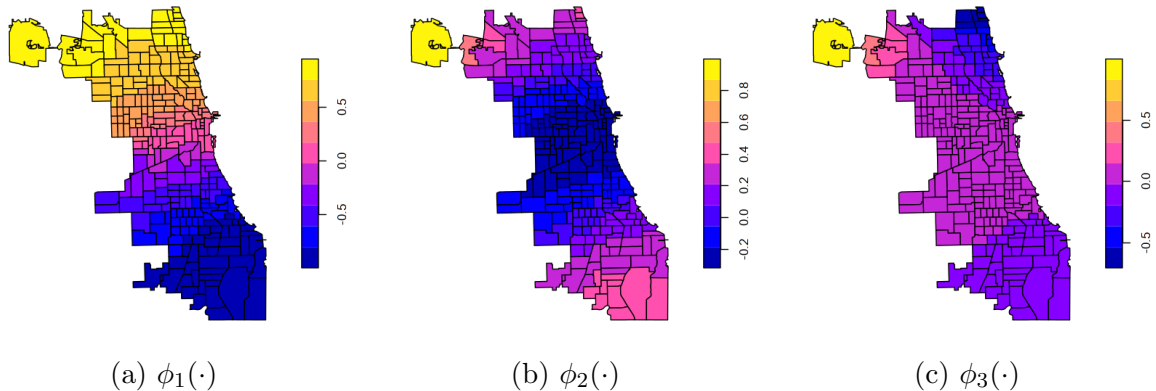


Figure 5: First three eigenvectors of the Laplacian are shown for the beat adjacency graph, mapped back to the geographic locations. All of the eigenvectors are normalized by the maximum absolute value. Notice spatial smoothness of the eigenvectors which is crucial to efficiently capturing horizontal variability of the data (i.e. distribution shifts over the graph). The boundaries of beats are shown based on the shape file from Chicago Data portal.

type and day, we capture the total count of that crime type for each beat; after normalizing this gives a daily probability distribution over the graph. Our goal is compare the collection of distributions of, say, theft occurring on Tuesday to those of Thursday and Saturday. The Tuesday versus Thursday comparison is intended as a null case, as we do not expect to see any differences between them [31].

We build the un-normalized Laplacian of the beat adjacency graph, and compute its lowest frequency $L = 20$ eigenvalues and eigenvectors. The first three eigenvectors are plotted in Figure 5. The number of inverse CDF values used in the embedding is $D' = 5$, which gives rise to $D = 100$ dimensional embedding. The results of comparisons are shown in the last two columns of Table 3; the p -values are obtained via the harmonic mean combination approach. We run the Benjamini-Hochberg [3] procedure on the 20 resulting p -values at the false discovery rate of 0.1, and the rejected hypotheses are indicated by the p -values in bold. As expected, no differences were detected between Tuesday and Thursday patterns. On the other hand, we see that there are statistically significant differences between Tuesday and Saturday patterns in the following categories of crime: theft, deceptive practice, battery, robbery, narcotics, and criminal damage.

Brain Connectomics In this example, we consider two publicly available brain connectomics datasets [1, 2] distributed as a part of the R package `graphclass`³. Both are based on resting state functional magnetic resonance imaging (fMRI): COBRE has data on 54 schizophrenics and 70 controls, and UMich with 39 schizophrenics and 40 controls. The datasets capture the pairwise correlations between 264 regions of interest (ROI) of Power parcellation [29] and can be considered as a 264 node graph (263 nodes for COBRE as ROI 75 is missing) with positive and negative edge weights.

We define three probability measures supported on the nodes of the graph. For each ROI we take the sum of absolute values of all its correlations with the remaining ROIs. Now we have a positive number assigned to each node capturing its overall connectivity to the rest of the graph and we normalize to obtain a measure; this construction will be referred to as “all correlations”.

³<http://github.com/jesusdaniel/graphclass>

Crime Type	Tuesday		Thursday		Saturday		Tue vs Thu	Tue vs Sat
	#Hists	count	#hists	count	#hists	count	<i>p</i> -value	<i>p</i> -value
Theft	52	178.7	52	182.9	52	180.2	0.428	4.2e-06
Deceptive Practice	51	55.8	52	54.9	52	44.4	0.313	0.001
Battery	52	125.8	52	123.0	52	154.9	0.430	0.001
Robbery	50	25.2	50	25.1	52	28.1	0.119	0.003
Narcotics	51	36.0	51	34.6	50	36.9	0.854	0.004
Criminal Damage	52	70.0	52	73.7	52	83.0	0.855	0.02
Other Offense	52	49.5	52	48.4	52	44.1	0.9c31	0.052
Burglary	52	34.0	52	33.1	52	29.1	0.142	0.261
Assault	52	57.2	52	59.3	52	52.4	0.997	0.38
Motor Vehicle Theft	52	27.9	52	26.2	51	28.1	0.858	0.416

Table 3: Results on Chicago Crime dataset. The entries in bold correspond to the rejected hypotheses with the BH procedure at the FDR level of 0.1.

Dataset	All correlations	Positive correlations	Negative correlations
COBRE	0.0045	0.00012	0.0019
UMich	0.549	0.132	0.028

Table 4: Comparison results between the schizophrenic and control groups for brain connectomics datasets.

Note that each scanned subject gives rise to a separate “all correlations” probability measure on the same underlying node set. The “positive correlations” and “negative correlations” constructions are based on keeping respectively only positive or only negative correlations and aggregating as above.

We also need a fixed base graph for the computation of the Laplacian eigen-decomposition; this graph should capture the spatial connectivity of the ROIs which is relevant due to the smooth nature of the blood oxygenation level dependent (BOLD) signal that is used for computing the correlations. To this end, we obtain the coordinates for the centers of the 264 ROIs⁴ and build the base graph by connecting each ROI to its nearest 8 ROIs. We compute the lowest frequency $L = 20$ eigenvalues and eigenvectors of the corresponding un-normalized Laplacian. The number of inverse CDF values used in the embedding is $D' = 5$, which gives rise to $D = 100$ dimensional embedding.

Table 4 shows the result of comparing the schizophrenic group to the control group for both of the datasets; the p -values are obtained via the harmonic mean combination approach. We can see that our approach detects statistically significant differences between the two groups in COBRE dataset in all of the three types of measures on graphs. In contrast, for UMich dataset, the difference is detected only in the negative correlations and is not as highly significant. This is potentially caused by the higher inhomogeneity of the UMich dataset that was pooled across five different experiments spanning seven years [2]. An interesting aspect of our analysis is that due to normalization (to obtain probability measures) the total sum of connectivity is factored out by the proposed method. As a result, the detected differences are not related to the well-known

⁴www.jonathanpower.net/2011-neuron-bigbrain.html

change in the overall connectivities between the two groups, but rather to distributional changes in marginal connectivity strengths.

6 Conclusion

We have introduced an approach for detecting differences in the average behavior of random collections of probability distributions. Our experiments confirm that the resulting tests are powerful and the p -values are well-calibrated. Several applications to real world data have been presented. Our approach is valid on general domains such as manifolds and graphs, thanks to the general nature of the Intrinsic Sliced 2-Wasserstein distance proposed in this paper.

Two straightforward developments have been omitted from our presentation to maintain the focus. First, given two collections of histograms on general domains one can test whether they were generated by the same process. This is similar to regular two-sample testing, except that our data points are histograms. For example, the Energy Distance based two sample test [33] can be adapted by replacing the Euclidean distance between points by ISW_2 between the histograms. The MMD-based test [17] can similarly be used in this setting, requiring a kernel function between histograms: we can use the Gaussian kernel where Euclidean distance is substituted by ISW_2 once again. The validity of both of these approaches hinge on Hilbertianity of pair-wise distances [28], which is satisfied by ISW_2 . Second, hypothesis tests to detect differences between three or more collections of histograms can be developed. Indeed, since our test is based on mean comparisons, under suitable assumptions we can instead of t -tests perform an ANOVA F -test for differences among means and combine the resulting p -values as before.

The construction of ISW_2 provides a novel embedding of probability distributions into a Hilbert space. This can be used to adapt even more of statistical methodology to very general spaces where the existence of Fréchet means or higher moments are not guaranteed. The ISW_2 can also be useful for machine learning applications where the prediction targets live in a general domain. Given that rigorous Fréchet mean-based methodology for such problems has only been proposed recently [9, 14, 22], development of prediction models for manifold-valued data that are free of restrictive assumptions is an attractive future line of research.

Acknowledgments

We would like to thank Paromita Dubey for providing source codes for the Fréchet ANOVA-based test. We are grateful to our colleagues from AT&T Mark Austin, James Klosowski, Deirdre Paul, Ann Skudlark, and Christopher Volinsky for their encouragement and support in exploring this research direction.

References

- [1] C. J. Aine, H. J. Bockholt, J. R. Bustillo, J. M. Cañive, A. Caprihan, C. Gasparovic, F. M. Hanlon, J. M. Houck, R. E. Jung, J. Lauriello, J. Liu, A. R. Mayer, N. I. Perrone-Bizzozero, S. Posse, J. M. Stephen, J. A. Turner, V. P. Clark, and Vince D. Calhoun. Multimodal neuroimaging in schizophrenia: Description and dissemination. *Neuroinformatics*, 15(4):343–364, Oct 2017.

- [2] Jesús D. Arroyo Reli3n, Daniel Kessler, Elizaveta Levina, and Stephan F. Taylor. Network classification with applications to brain connectomics. *Ann. Appl. Stat.*, 13(3):1648–1677, 09 2019.
- [3] Yoav Benjamini and Yocef Hochberg. Controlling the false discovery rate: A practical and powerful approach to multiple testing. *Journal of the Royal Statistical Society. Series B (Methodological)*, 57(1):289–300, 1995.
- [4] Bigot, J3r3mie. Statistical data analysis in the wasserstein space. *ESAIM: ProcS*, 68:1–19, 2020.
- [5] Patrick Billingsley. *Probability and measure*. Wiley, New York, third edition, 1995.
- [6] Brett Borden and James Luscombe. *Essential Mathematics for the Physical Sciences*, volume Volume I: Homogeneous boundary value problems, Fourier methods, and special functions, chapter Spherical harmonics and friends. Morgan & Claypool Publishers, 2017. Pages 6–1 to 6–26.
- [7] Elsa Cazelles, Vivien Seguy, J3r3mie Bigot, Marco Cuturi, and Nicolas Papadakis. Geodesic pca versus log-pca of histograms in the wasserstein space. *SIAM Journal on Scientific Computing*, 40(2):B429–B456, 2018.
- [8] Villani C3dric. *Topics in optimal transportation*. Graduate studies in mathematics. American mathematical society, Providence, Rhode Island.
- [9] Yaqing Chen, Zhenhua Lin, and Hans-Georg M3ller. Wasserstein regression, 2020.
- [10] Ronald R. Coifman and St3phane Lafon. Diffusion maps. *Applied and Computational Harmonic Analysis*, 21(1):5 – 30, 2006. Special Issue: Diffusion Maps and Wavelets.
- [11] J. Cremers and I. Klugkist. One Direction? A Tutorial for Circular Data Analysis Using R With Examples in Cognitive Psychology. *Frontiers in Psychology*, 9(2040):1–13, 2018.
- [12] Xiongtao Dai and Hans-Georg M3ller. Principal component analysis for functional data on riemannian manifolds and spheres. *Ann. Statist.*, 46(6B):3334–3361, 12 2018.
- [13] Paromita Dubey and Hans-Georg M3ller. Fr3chet analysis of variance for random objects. *Biometrika*, 106(4):803–821, 10 2019.
- [14] Gajardo, 3lvaro and Hans-Georg M3ller. Point Process Regression. <https://arxiv.org/abs/2006.00447>, 2020.
- [15] I. J. Good. Significance tests in parallel and in series. *Journal of the American Statistical Association*, 53(284):799–813, 1958.
- [16] T. Gorecki and L. Smaga. A Comparison of Tests for the One-Way ANOVA Problem for Functional Data. *Computational Statistics*, 30:987–1010, 2015.
- [17] Arthur Gretton, Karsten M. Borgwardt, Malte J. Rasch, Bernhard Sch3lkopf, and Alexander Smola. A kernel two-sample test. *J. Mach. Learn. Res.*, 13:723–773, March 2012.
- [18] Jingchen Hu, Yiqian Shi, and Bin Xu. The gradient estimate of a neumann eigenfunction on a compact manifold with boundary. *Chinese Annals of Mathematics, Series B*, 36(6):991–1000, Nov 2015.

- [19] S. Iloga, O. Romain, and M. Tchuente. An accurate HMM-based similarity measure between finite sets of histograms. *Pattern Analysis and Applications*, 22:1079–1104, 2019.
- [20] Soheil Kolouri, Kimia Nadjahi, Umut Simsekli, Roland Badeau, and Gustavo Rohde. Generalized sliced wasserstein distances. In H. Wallach, H. Larochelle, A. Beygelzimer, F. Alché-Buc, E. Fox, and R. Garnett, editors, *Advances in Neural Information Processing Systems 32*, pages 261–272. Curran Associates, Inc., 2019.
- [21] Soheil Kolouri, Phillip E. Pope, Charles E. Martin, and Gustavo K. Rohde. Sliced wasserstein auto-encoders. In *7th International Conference on Learning Representations, ICLR 2019, New Orleans, LA, USA, May 6-9, 2019*. OpenReview.net, 2019.
- [22] Kyunghee Han and Hans-Georg Müller and Byeong U. Park. Additive functional regression for densities as responses. *Journal of the American Statistical Association*, 115:997–1010, 2020.
- [23] Yaron Lipman, Raif M. Rustamov, and Thomas A. Funkhouser. Biharmonic distance. *ACM Trans. Graph.*, 29(3), July 2010.
- [24] Yaowu Liu and Jun Xie. Cauchy combination test: A powerful test with analytic p-value calculation under arbitrary dependency structures. *Journal of the American Statistical Association*, 115(529):393–402, 2020.
- [25] Charles A. Micchelli, Yuesheng Xu, and Haizhang Zhang. Universal kernels. *J. Mach. Learn. Res.*, 7:2651–2667, December 2006.
- [26] Victor M. Panaretos and Yoav Zemel. Statistical aspects of wasserstein distances. *Annual Review of Statistics and Its Application*, 6(1):405–431, 2019.
- [27] Alexander Petersen and Hans-Georg Müller. Functional data analysis for density functions by transformation to a hilbert space. *Ann. Statist.*, 44(1):183–218, 02 2016.
- [28] Gabriel Peyré and Marco Cuturi. Computational optimal transport: With applications to data science. *Foundations and Trends in Machine Learning*, 11(5-6):355–607, 2019.
- [29] Jonathan D. Power, Alexander L. Cohen, Steven M. Nelson, Gagan S. Wig, Kelly Anne Barnes, Jessica A. Church, Alecia C. Vogel, Timothy O. Laumann, Fran M. Miezin, Bradley L. Schlaggar, and Steven E. Petersen. Functional network organization of the human brain. *Neuron*, 72(4):665–678, Nov 2011. 22099467[pmid].
- [30] M. L. Rizzo and G. J. Székely. DISCO analysis: A nonparametric extension of analysis of variance. *Ann. Appl. Stat.*, 4:1034–1055, 2010.
- [31] Raif M. Rustamov and James T. Klosowski. Kernel mean embedding based hypothesis tests for comparing spatial point patterns. *Spatial Statistics*, 38:100459, 2020.
- [32] Justin Solomon, Raif M. Rustamov, Leonidas J. Guibas, and Adrian Butscher. Wasserstein propagation for semi-supervised learning. In *Proceedings of the 31th International Conference on Machine Learning, ICML 2014, Beijing, China, 21-26 June 2014*, volume 32 of *JMLR Workshop and Conference Proceedings*, pages 306–314. JMLR.org, 2014.
- [33] Gábor J. Székely and Maria L. Rizzo. A new test for multivariate normality. *Journal of Multivariate Analysis*, 93(1):58 – 80, 2005.

- [34] Jane-Ling Wang, Jeng-Min Chiou, and Hans-Georg Müller. Functional data analysis. *Annual Review of Statistics and Its Application*, 3(1):257–295, 2016.
- [35] Daniel J. Wilson. The harmonic mean p-value for combining dependent tests. *Proceedings of the National Academy of Sciences*, 116(4):1195–1200, 2019.
- [36] C. Zhang, H. Peng, and J.-T. Zhang. Two Samples Tests for Functional Data. *Communications in Statistics–Theory and Methods*, 39:559–578, 2010.
- [37] J.-T. Zhang. *Analysis of Variance for Functional Data*. Chapman and Hall/CRC, first edition, 2013.
- [38] J.-T. Zhang, M.-Y. Chen, H.-T. Wu, and B. Zhou. A new test for functional one-way ANOVA with applications to ischemic heart screening. *Computational Statistics & Data Analysis*, 132:3–17, 2019.

Appendix

Additional numerical results

Table 5 shows the outputs for Cauchy p -value combination tests, and other 8 competing methods from the R package `fdANOVA` for the functional curves synthetic data setting in Section 5.1. See <https://www.rdocumentation.org/packages/fdANOVA/versions/0.1.2/topics/fanova.tests> for full names of all methods above.

δ	CH	CS	L2N	L2b	FN	FB	Fb	GPF	ISD	cauchy	Cauchy
0	0.02	0.023	0.026	0.02	0.024	0.043	0.016	0.03	0.037	0.045	0.045
0.1	0.024	0.024	0.029	0.026	0.028	0.048	0.021	0.034	0.045	0.045	0.055
0.2	0.035	0.038	0.039	0.039	0.039	0.051	0.028	0.036	0.042	0.042	0.071
0.3	0.03	0.035	0.04	0.036	0.037	0.053	0.026	0.039	0.054	0.054	0.094
0.4	0.045	0.05	0.049	0.051	0.048	0.076	0.04	0.055	0.071	0.071	0.145
0.5	0.063	0.069	0.065	0.069	0.065	0.091	0.062	0.072	0.098	0.098	0.19
0.6	0.065	0.087	0.081	0.084	0.079	0.121	0.064	0.092	0.136	0.136	0.264
0.7	0.093	0.105	0.107	0.108	0.104	0.142	0.094	0.117	0.198	0.198	0.346
0.8	0.125	0.146	0.14	0.15	0.137	0.19	0.123	0.157	0.218	0.218	0.422
0.9	0.156	0.185	0.174	0.188	0.173	0.218	0.162	0.188	0.282	0.282	0.504
1	0.222	0.267	0.252	0.272	0.245	0.316	0.237	0.274	0.368	0.368	0.6
1.1	0.269	0.323	0.306	0.324	0.3	0.371	0.275	0.336	0.464	0.464	0.685
1.2	0.337	0.379	0.363	0.376	0.357	0.423	0.35	0.406	0.515	0.515	0.745
1.3	0.441	0.487	0.475	0.487	0.47	0.522	0.458	0.492	0.576	0.576	0.831
1.4	0.525	0.574	0.547	0.58	0.544	0.614	0.54	0.581	0.646	0.646	0.859
1.5	0.597	0.643	0.62	0.649	0.616	0.684	0.611	0.647	0.702	0.702	0.91
1.6	0.672	0.735	0.701	0.732	0.698	0.764	0.696	0.734	0.77	0.77	0.944
1.7	0.744	0.793	0.768	0.796	0.763	0.819	0.763	0.785	0.809	0.809	0.964
1.8	0.814	0.848	0.832	0.85	0.83	0.862	0.829	0.847	0.834	0.834	0.964
1.9	0.866	0.898	0.885	0.899	0.884	0.908	0.883	0.894	0.877	0.877	0.975
2	0.899	0.923	0.909	0.926	0.908	0.939	0.912	0.924	0.906	0.906	0.984
2.1	0.932	0.946	0.941	0.947	0.941	0.96	0.94	0.946	0.921	0.921	0.984
2.2	0.951	0.966	0.958	0.967	0.957	0.973	0.959	0.963	0.931	0.931	0.994
2.3	0.962	0.979	0.968	0.977	0.966	0.982	0.969	0.97	0.941	0.941	0.99
2.4	0.979	0.989	0.983	0.989	0.983	0.99	0.985	0.981	0.97	0.97	0.995
2.5	0.987	0.989	0.987	0.988	0.987	0.991	0.987	0.988	0.976	0.976	0.995
2.6	0.989	0.993	0.99	0.993	0.989	0.993	0.991	0.991	0.979	0.979	0.998
2.7	0.994	0.995	0.994	0.995	0.994	0.995	0.994	0.994	0.978	0.978	0.998
2.8	0.994	0.995	0.994	0.995	0.994	0.996	0.994	0.995	0.988	0.988	0.998
2.9	0.995	0.997	0.996	0.996	0.995	0.998	0.997	0.996	0.991	0.991	1
3	0.999	1	1	1	1	1	1	0.999	0.993	0.993	0.999

Table 5: Outputs for other methods in the functional curves synthetic data setting.